Improved Experimental Method for Measuring Gas Diffusivity Through Thin Porous Media

Grant Unsworth, Lu Dong, and Xianguo Li
20/20 Laboratory for Fuel Cell and Green Energy RD&D, Dept. of Mechanical and Mechatronics Engineering, University of Waterloo, Waterloo, ON Canada N2L 3G1

DOI 10.1002/aic.13911
Published online September 11, 2012 in Wiley Online Library (wileyonlinelibrary.com).

Gas diffusion through porous media is critical for the high current density operation of a polymer electrolyte membrane fuel cell, where the electrochemical reaction becomes rate limited by the diffusive flux of reactants. Precise knowledge of the diffusivity through various components in a fuel cell is necessary for accurate modeling and analysis. However, many experimental measurements of diffusivity in literature have high measurement uncertainty. In this study, an improvement to the accuracy of the Loschmidt cell method is presented for measuring the diffusivity through materials with a submillimeter thickness. The diffusivity through various gas diffusion layers (GDLs) is measured, and the relative differences between GDLs are explained using scanning electron microscopy and the method of standard porosimetry. The experimental results from this study and others in current literature are used to develop a generalized correlation for the diffusibility as a function of porosity in the through-plane direction of GDLs. © 2012 American Institute of Chemical Engineers *AIChE J,* 59: 1409–1419, 2013

Keywords: polymer electrolyte membrane fuel cell, gas diffusion layer, Loschmidt cell, closed-tube method, effective diffusion coefficient, experimental measurement, porous media

Introduction

The measurement and correlation of fluxes for gas diffusion through thin porous media is of considerable importance to the development of the polymer electrolyte membrane fuel cell (PEMFC). Reactants and products must both pass through the porous gas diffusion layer (GDL) that connects flow channels to the active catalyst surface where the electrochemical reaction occurs. Diffusion is considered the primary mode of transport for delivery of reactants,[1] and at high current densities the electrochemical reaction becomes rate limited by the diffusive flux through the GDL. A thorough understanding of how the GDL microstructure and operating conditions affect the diffusive flux can lead to improvements in GDL design. However, mass transport through the GDL is highly complex and difficult to model. Gas diffusion is governed by molecular diffusion, while Knudsen, viscous, and nonequimolar diffusion can occur near walls of the porous media.[2] In addition, the pore structure is nonuniform with a broad range of pore sizes and shapes.

In general, macroscopic properties of the GDL are easy to measure. For example, pore size may be determined by modern techniques such as standard porosimetry,[3] mercury porosimetry, atomic force microscopy, and scanning electron microscopy (SEM). However, none of the methods are able to determine the shape or effective length of the pores. The GDL is a highly porous (> 70%) anisotropic material typically made up of graphitized carbon fibers. The fibers may be manufactured into either a carbon paper of random fibers held together with a carbonized thermoset resin binder or a carbon cloth of woven fibers without any binder. This study focuses on the former, while the methods used in this article could also be applied to the later.

Pure gas diffusion for a binary gas system is governed by Fick's Second Law as follows,

$$\frac{\partial C_{\mathrm{i}}}{\partial t} = D_{\mathrm{ij}} \nabla^2 C_{\mathrm{i}} \tag{1}$$

where C_{i} is the concentration of the gaseous species i and D_{ij} is the diffusion coefficient between species i and j. Flow through porous media, such as the GDL, are often described by modifying Fick's law with an effective diffusion coefficient, $D_{\mathrm{ij}}^{\mathrm{eff}}$, that takes into account the obstruction that the GDL has on the flow, such that,

$$D_{\mathrm{ij}}^{\mathrm{eff}} = f(\epsilon, \tau) D_{\mathrm{ij}} = \frac{\epsilon}{\tau} D_{\mathrm{ij}} \tag{2}$$

where $f(\epsilon, \tau)$ is the diffusibility, ϵ is the porosity, and τ is the tortuosity. The adjustable parameter tortuosity is included to account for the shape, orientation, and effective length of the pores. It is defined as the length of a "tortuous" path divided by the straight-line distance through a porous structure. However, tortuosity cannot be readily measured. Thus, the diffusibility, $f(\epsilon, \tau)$, is often estimated by many geometric models as a function of only ϵ.[4] The most well-known correlation in PEMFC literature is that by Bruggeman,[5]

Correspondence concerning this article should be addressed to X. Li at xianguo.li@uwaterloo.ca.

$$f(\epsilon,\tau) \approx f(\epsilon) = \epsilon^{1.5} \tag{3}$$

The shortcoming of the Bruggeman correlation is that it was developed from a geometric model of spherical particles, a significant departure from the geometry of a GDL. Das et al.[6] acknowledges this limitation while formulating a mathematical model for GDL diffusivity based on the Hashin coated sphere model

$$f(\epsilon,\tau) \approx f(\epsilon) = \left(1 - \lambda_g\left(\frac{3(1-\epsilon)}{3-\epsilon}\right)\right) \tag{4}$$

where λ_g is a geometric factor that accounts for the fibrous geometry of GDLs and must be estimated using an appropriate experimental scheme. Zamel et al.[7] used a numerical simulation of the diffusion process through a three-dimensional (3D) representation of a GDL to generate an expression for the geometric factor, of the form

$$\lambda_g = \epsilon A \cosh(B\epsilon - C) \tag{5}$$

where A, B, and C are constants. On the other hand, Tomadakis and Sotirchos[8,9] proposed the following correlation based on a model of random cylindrical fibers

$$f(\epsilon,\tau) \approx f(\epsilon) = \frac{0.9126}{\epsilon(\epsilon - 0.11)^{0.785}} \tag{6}$$

Unfortunately, experimental measurements[10–13] have suggested that many of these correlations for porous media significantly over predict D_{ij}^{eff} in the GDL. This is a considerable issue for numerical studies that model PEMFC performance using these correlations, especially at high current density conditions where reaction rate is limited by mass transport.

To develop a more appropriate correlation, a number of studies have focused on experimentally measuring the diffusion coefficient through commercially available GDLs. Baker et al.[14,15] and others[16,17] made *in situ* limiting current measurements to characterize gas transport resistance in an operating PEMFC. They were able to separate the effect of the GDL on the overall gas transport resistance in the cell; however, it was not possible to distinguish between in-plane and through-plane diffusion, variations in compression by the bipolar plates, and mass transfer due to convection. In another study, Baker et al.[14] was able to isolate these parameters by measuring water vapor diffusion with an *ex situ* apparatus. The simple technique involved measuring the evaporation rate of water through a GDL, which is a function of the diffusibility of the GDL. However, this method required at least 24 h to perform one measurement, limiting the practical number of operating conditions and sample GDLs that could be evaluated. Kramer et al.[10] and others[12,18,19] used electrochemical diffusimetry, a novel analogy between electrical resistance and gas diffusion, to determine ϵ/τ in a GDL. Their results compared well with Baker *et al.*[14] at compressions of less than 25%. However, the primary limitation of this method is that diffusibility of the GDL is inferred rather than directly measured. Furthermore, electrochemical diffusimetry may not be appropriate for quantifying diffusion in the pores of the microporous and catalyst layers of the PEMFC, regions where Knudsen diffusion dominates and the relation between Fick's law and Ohm's law is no longer valid. This limits the usefulness of this technique beyond GDL. LaManna et al.[13] used a parallel flow mass exchanger to measure vapor diffusion rates across various GDLs with a stated uncertainty of 22%. Although the sources of the uncertainty are not discussed, operating the inlet gas stream at 95% relative humidity and 25°C can lead to large errors in relative humidity measurements from temperature variations on the order of (10^{-1})°C. More accurate measurements could be achieved by operating the apparatus at 80°C, a temperature where the air holds significantly more water vapor and small temperature changes have less effect on relative humidity. Zamel et al.[11] and a similar study by Chan et al.[20] modified a Loschmidt cell, normally used to evaluate binary gas diffusion coefficients, to measure the diffusive flux through a GDL. The Loschmidt cell directly measures gas concentration and is simple in design, requiring only limited assumptions. The measurement system has the potential to provide more accurate measurements than other discussed techniques, and has already been well demonstrated for binary gas systems.[21]

The experimental uncertainty in the GDL diffusivity measurements conducted by Zamel et al.[11] is large, as will be shown, and grows exponentially large for the measurement of thinner materials pertinent to the development of PEMFCs such as the microporous layer[20] and catalyst layer.[22] This study builds upon the work by Dong et al.,[23] who determined the theoretical accuracy of measuring diffusivity of porous media with the Loschmidt cell method, with the design of a new Loschmidt cell that can measure submillimeter thick materials such as the gas diffusion ($\sim$200 μm), microporous ($\sim$50 μm), and catalyst layers ($\sim$10 μm) with a high level of accuracy. The improved accuracy is achieved by analysing design parameters in the Loschmidt cell that are sensitive to measurement error and have the largest contribution to measurement uncertainty. The new Loschmidt cell is used to measure the diffusibility of three commercially available GDLs in this study. The structure and properties of the GDLs are assessed using SEM and the method of standard porosimetry (MSP), which are compared with the diffusibility results gathered from the Loschmidt cell. Diffusibility measurements from several research groups using a variety of measurement techniques are presented in a comprehensive comparison. This exercise is done to assess the range of quoted values in literature, and to determine whether there is a consensus on diffusibility values for a specific GDL. Using these comparisons, a correlation for GDL diffusibility is developed based on the measurements from numerous experimental studies, which can be used for high accuracy modeling and analysis of PEMFCs operating at high current densities.

Experimental

Apparatus and Measurement Principle

Loschmidt developed the closed-tube method in 1870.[24] As a result, an experimental apparatus using the closed-tube method is commonly referred to as a Loschmidt cell. Diffusive flux is determined through mixture composition measurements in the Loschmidt cell, which are a function of both time and position in a long tube that is closed at both ends. Primary assumptions for this method are that diffusion occurs in 1D, the cell has a uniform cross section, and it is symmetrical about its midplane. It is also assumed that the diffusion coefficient is independent of concentration, which varies with time due to the transient nature of the method. For gases, this is generally true.[25]

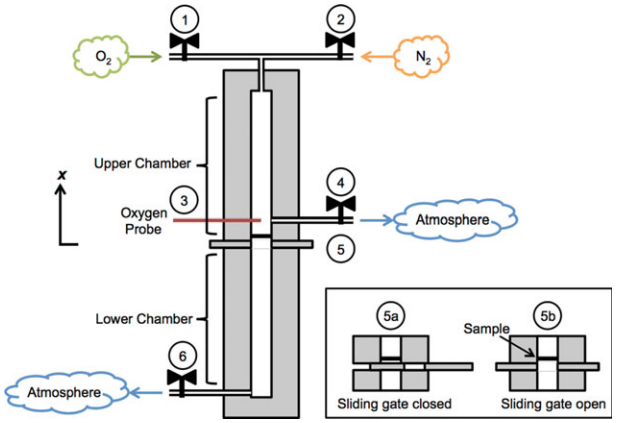

Figure 1. Modified Loschmidt cell used in the present study.

[Color figure can be viewed in the online issue, which is available at wileyonlinelibrary.com.]

The Loschmidt cell must be modified to measure gas diffusion through porous media by allowing a sample to be placed near the midpoint of the long tube. A schematic of the apparatus used in this study is provided in Figure 1, whose design is an evolution of the modified Loschmidt cell in literature.[11,20,22,26–29] Different gas species are contained in the upper and lower chambers of the cell separated by a sliding gate (5a), in this study nitrogen and oxygen, respectively. When the sliding gate is opened (5b), the gas species diffuse together through a sample placed at the interface between the two chambers. The oxygen concentration at a known point in the cell is measured as a function of elapsed time using an Ocean Optics FOXY-AL300 oxygen sensor.

Performing a diffusion measurement begins by purging the cell with oxygen from inlet (1) and venting it to atmosphere at outlet (6) until the oxygen probe (3) stabilizes at 100% oxygen for a prolonged period of time. The sliding gate (5) is then closed to seal off the bottom chamber. Next, the upper chamber is purged with nitrogen from inlet (2) while venting it to atmosphere at outlet (4) until the oxygen concentration stabilizes at 0% for a prolonged period of time. Failure to achieve the exact 100 and 0% oxygen concentration set points at the oxygen probe (3) indicates a problem with the apparatus that could be related to mechanical sealing, oxygen probe calibration, or a software logic error. This provides a level of automated fault checking that is an improvement from the purging method described in previous studies.[11,26,28] The diffusion measurement proceeds by opening the sliding gate (5b) and monitoring oxygen concentration over a set period of time. The length of time required is discussed in the complementary study by Dong et al.[23] A typical set of data collected by the oxygen probe at 0.5 s intervals is provided in Figure 2 for an experiment involving a Toray TGP-H-120 GDL at 50°C.

Oxygen sensor and phase fluorometry

The diffusive flux through the Loschmidt cell is calculated from the oxygen concentration measurements of a single-oxygen sensor probe. Thus, its calibration and measurement accuracy are paramount for achieving precise results. Through a measurement technique known as phase fluorometry, the oxygen sensor measures fluorescence quenching by oxygen molecules and correlates it to the partial pressure of an oxygen mixture. A luminophore (in this case ruthenium) tipped probe fluoresces when it is excited by a blue (470 *nm*) LED source.[30] The florescence is quenched through a transfer of energy when a molecule of oxygen physically collides with a fluorophore in its excited state. Unlike nitrogen and other molecules found in air, oxygen is uniquely able to quench the fluorescence of certain luminophores because it is a triplet molecule.[31] The remaining light energy is passed through the probe along an optical fiber to a spectrometer. Lifetime, κ, is calculated from the measured phase shift, ϕ, between the excitation LED and the fluorescence emission, and the frequency of the light, f, using the following formula,

$$\kappa = \frac{1}{2\pi f}\tan(\phi) \tag{7}$$

The amount of fluorescence quenching depends on the rate of collisions, and therefore, the concentration (or partial pressure) of oxygen in the cell. By extension, the measurements are sensitive to the absolute pressure and temperature of the gas mixture. Thus, regular calibration is necessary to account for daily fluctuations in atmospheric pressure and design temperature set points.

Exposing the oxygen sensor to a series of known oxygen concentrations allows the sensor to be calibrated. The nitrogen-oxygen gas composition is controlled by two Omega FMA-series mass flow controllers that feed the correct ratio of oxygen and nitrogen through inlets (1) and (2), past the oxygen sensor, and out through outlet (4) in Figure 1. A 20-point calibration (typical of Figure 3) is automatically performed before each set of runs to correlate measured κ values to oxygen concentration. A high-order polynomial fit is applied to the data points to smooth the data, and to enable interpolation of other κ values.

Sensor drift is the largest concern for this type of measurement system. The manufacturer of the oxygen sensor lists the stability of the oxygen measurement as decreasing by 0.01% per hour at continuous operation. The drift is practically eliminated by recalibrating the probe before each set of measurements using an automated process.

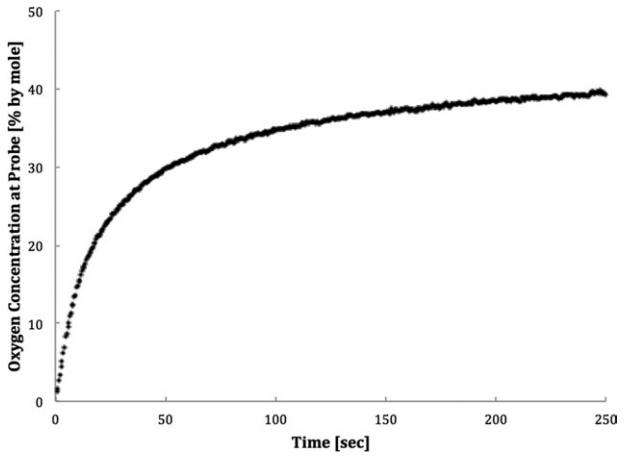

Figure 2. Oxygen concentration vs. time measured by the oxygen sensor for an experiment involving a Toray TGP-H-120 gas diffusion layer at 50°C.

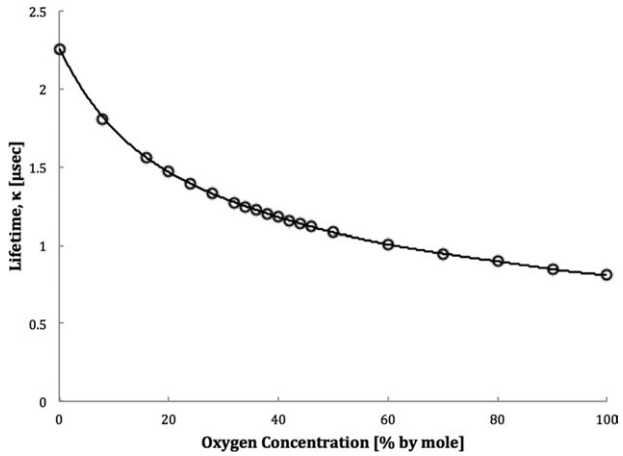

Figure 3. Typical calibration curve for oxygen sensor relating lifetime to oxygen concentration.

Temperature

The temperature at which the diffusion experiment takes place is controlled by a temperature-controlled water loop that circulates through passages machined adjacent to the gas column in the Loschmidt cell, depicted in Figure 4. A Thermo Scientific RTE-7 temperature bath maintains temperature stability to within 0.2°C. Manifolds on the hot and cold side of the loop ensure even flow through each passage in the Loschmidt cell and, thus, an equal temperature distribution. A new calibration is required for each temperature set point, because the oxygen concentration measurement is sensitive to absolute temperature. Thermocouples located in the upper and lower gas chambers confirm gas temperature uniformity throughout the duration of a test. The maximum operating temperature of the probe is rated at 80°C. Measurements were conducted over a range of temperatures (25, 50, and 70°C) designed to simulate conditions that are typical of an operating PEM fuel cell.

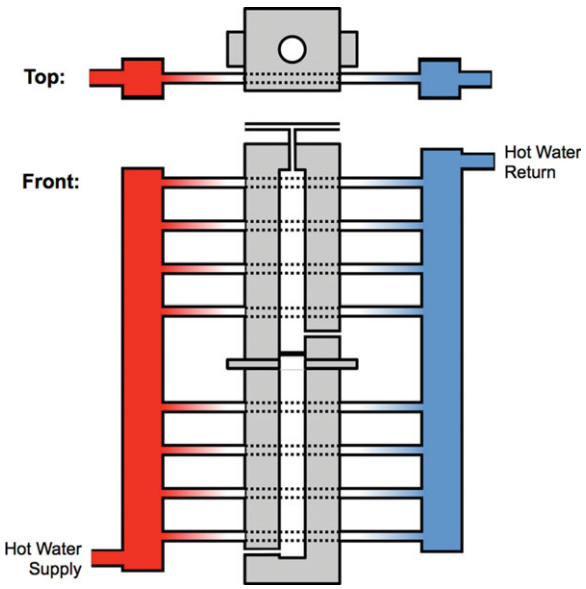

Figure 4. Schematic of temperature controlled water loop for the Loschmidt cell used in the present study.

[Color figure can be viewed in the online issue, which is available at wileyonlinelibrary.com.]

Table 1. Properties of Gas Diffusion Layers used in the Present Work

	Thickness (μm)	Porosity
Toray TGP-H-060	196	0.785
Toray TGP-H-120	364	0.769
SolviCore Type A	194	0.844

Gas diffusion layer

The properties of the GDL used in this study are summarized in Table 1. Thickness was determined by taking the average micrometer readings of three samples measured at five locations per sample. Porosity was determined from an average of three samples each measured once using the MSP technique (Porotech, Toronto, ON). Thickness and porosity measurements were found to be within 3% of the manufacturer's specifications for Toray GDL.[32] SolviCore did not provide similar information.

The GDLs were selected so that thickness (Toray TGP-H-60 and TGP-H-120) and manufacturer (Toray and SolviCore) variations could be compared. Although treating GDLs with a hydrophobic agent such as polytetrafluoroethylene (PTFE) is typical in commercial PEMFCs, raw GDLs were intentionally chosen to simplify the study between pore structure and gaseous diffusion. In an operating PEMFC, both compression and liquid water saturation alter the porosity of the GDL and impact diffusivity. The experimental method developed in this study could be applied to measure the effect of these variables on diffusivity.

Gas diffusion measurements were conducted using three samples of each type of GDL. Variability in results for the same type of GDL were within the bounds of experimental uncertainty described in the following section. Each sample was tested three times. Each test consisted of 20 experimental runs performed consecutively with the same calibration. To observe the effects of temperature, these tests were repeated over three temperatures of 25, 50, and 70°C. Binary gas diffusion measurements were performed in a similar manner. Results for each GDL were averaged using a 95% confidence interval.

Data Analysis

Fick's Second Law for 1D gas diffusion with constant diffusivity, as given in Eq. 1, can be solved for the Loschmidt cell using separation of variables and applying the following initial and boundary conditions

$$\left.\frac{\partial C}{\partial x}\right|_{\pm L/2} = 0 \tag{8}$$

$$C(-L/2 \le x < 0, t = 0) = C_{o,b} \tag{9}$$

$$C(0 < x \le L/2, t = 0) = C_{o,t} \tag{10}$$

where L is the total length of the Loschmidt cell, $C_{o,b}$ is the initial concentration in the bottom chamber, and $C_{o,t}$ is the initial concentration in the top chamber. An analytical solution for gas diffusion in the Loschmidt cell is obtained as follows,[33]

$$C(x,t) = \frac{C_{o,b} + C_{o,t}}{2} - (C_{o,b} - C_{o,t})\frac{2}{\pi}\sum_{m=0}^{\infty}\frac{e^{-\left(\frac{\pi}{L}\right)^2(2m+1)^2 D_{ij}t}}{2m+1} \sin\frac{\pi x}{L}(2m+1) \tag{11}$$

where C is the concentration at any location x and time t and D_{ij} is an estimate of the diffusion coefficient. The curve

generated by the analytical solution, Eq. 11, using an initially assumed diffusivity is compared to the measured oxygen concentration as a function of time, such as the one shown in Figure 3. The difference is measured in terms of a root-mean-squared (RMS) error defined as,

$$\mathrm{RMS}(D_{ij}) = \left(\frac{1}{p} \sum_{n=1}^{p} \left[\eta(x_p, t_n) - \eta_n \right]^2 \right)^{1/2} \tag{12}$$

where p is the total number of points considered (typically 500 in this study), x_p is the location of the oxygen probe, t_n is the time of measurement n, and η_n is the concentration of measurement n. This expresses how well the assumed diffusion coefficient fits the data. An accurate estimate of the diffusion coefficient is found by applying the Newton–Raphson method to find successively better approximations for D_{ij}. Because the derivatives for RMS are not easily found, finite difference approximations for the first and second derivatives can be expressed as

$$\mathrm{RMS}'(D_{ij}) \approx \frac{\mathrm{RMS}(D_{ij} + rD_{ij}) - \mathrm{RMS}(D_{ij} - rD_{ij})}{2rD_{ij}} \tag{13}$$

$$\mathrm{RMS}''(D_{ij}) \approx \frac{\mathrm{RMS}(D_{ij}+rD_{ij}) - 2\mathrm{RMS}(D_{ij}) + \mathrm{RMS}(D_{ij} - rD_{ij})}{(rD_{ij})^2} \tag{14}$$

The ratio r is used rather than a constant ΔD so that the magnitude of the change for each step is related to the magnitude of D_{ij}. This ensures stability even with significant changes in order of magnitude. From Eqs. 13 and 14, the Newton–Raphson iteration $k + 1$ with a relaxation term, ω, can be written as a function of the previous iteration k, such that

$$D_{ij}^{k+1} \approx D_{ij}^{k} - (1 - \omega) \left[\frac{\mathrm{RMS}'(D_{ij}^{k})}{\mathrm{RMS}''(D_{ij}^{k})} \right] \tag{15}$$

This process is executed in Matlab until solution convergence for the binary gas diffusion coefficient, D_{ij}, where the criterion for convergence is

$$D_{ij}^{k+1} - D_{ij}^{k} \leq (0.1\%) D_{ij}^{k} \tag{16}$$

The error generated from Eq. 16 is deemed to have a negligible effect on D_{ij}, considering the experimental error that is discussed in the following section is one order of magnitude larger.

When a porous sample is inserted into the Loschmidt cell, Eq. 15 produces an equivalent diffusion coefficient, D_{ij}^{eq}, that represents the heterogeneous diffusion through the bulk gas and the sample. Following the procedure used in previous studies,[11,20,22,27,29] the resistance network method may be applied between the oxygen probe (3) and sliding gate interface (5) in Figure 1 in order to solve for the effective diffusion coefficient of the porous sample. The equivalent diffusive resistance, R_{eq}, is the sum of the diffusive resistance through the binary gas, R_{binary}, and the sample, R_{eff}

$$R_{eq} = R_{binary} + R_{eff} \tag{17}$$

or,

$$\frac{x_p}{D_{ij}^{eq}} = \frac{x_p - l}{D_{ij}^{binary}} + \frac{l}{D_{ij}^{eff}} \tag{18}$$

where l is the thickness of the porous sample. The validity of solving for R_{eff} with the resistance network method has not been discussed in previous studies.[11,20,22,27,29] Dong et al.[23] demonstrates that the method is only accurate within a specific range of Fourier numbers

$$Fo = \frac{D_{ij} t}{{x_p}^2} \tag{19}$$

where t is the characteristic time, or the length of time the experiment is run for (see Figure 2). The Fourier number can be controlled for a specific experiment by adjusting t.

Uncertainty Analysis

The diffusion coefficient, D_{ij}, is not measured directly by the experimental apparatus. Rather, D_{ij} is calculated from a set of measurements, X_N, as described earlier, such that

$$D_{ij} = D_{ij}(X_1, X_2, \ldots, X_N) \tag{20}$$

A traditional method of calculating the uncertainty of D_{ij} is through a root-sum-square (RSS) method where each term is the partial derivative of D_{ij} with respect to X_n multiplied by the known uncertainty interval of X_n, or

$$\delta D_{ij} = \left[\sum_{n=1}^{N} \left(\frac{\partial D_{ij}}{\partial X_n} \delta X_n \right)^2 \right]^{1/2} \tag{21}$$

However, D_{ij} is not easily differentiable considering the iterative nature of the solution described in Section Data Analysis. For such a case, Moffat[34] recommends a computerized uncertainty analysis where input variables are sequentially perturbed to generate an uncertainty contribution in D_{ij} for each variable. The overall uncertainty in the result is the RSS of these individual contributions.

Sources of uncertainty in the measurement apparatus that have a significant impact on the measured diffusion coefficient include the oxygen sensor and the oxygen and nitrogen mass flow controllers.

The manufacturer of the oxygen sensor quotes the uncertainty as less than 5% of reading for oxygen concentrations in the range of 0–20%. However, calculation of the diffusion coefficient is most sensitive to the measured oxygen concentrations from 20 to 40%. Without a clear measure of uncertainty from the manufacturer, the mass flow controllers feeding oxygen and nitrogen into the cell are used to evaluate the accuracy of the sensor. Based on repeated measurements, the oxygen sensor is found to have an error of less than 1% of full scale when the mass flow controllers supply a gas mixture with a known concentration of oxygen. The uncertainty of the oxygen sensor is taken as $\pm 1\%$ of full scale for the purposes of this analysis.

The performance of the oxygen sensor is dependent on its calibration at a specific temperature and pressure and is also necessary to compensate for sensor drift over time. Mass flow controllers flow oxygen and nitrogen past the oxygen sensor to calibrate it to a series of known concentrations.

Table 2. Sources of Measurement Equipment Uncertainty in the Experimental Apparatus and their Impact on the Uncertainty of the Calculated Diffusion Coefficient

Source of Uncertainty	Measurement Error (% of full scale)	Uncertainty in D_{ij} (%)
Oxygen sensor measurement	1.0	0.69
Mass flow controller measurement	1.0	2.2

The manufacturer provides an uncertainty of $\pm 1.0\%$ of full scale for each mass flow controller.

Table 2 provides the results of a computerized uncertainty analysis that was performed on the two major sources of uncertainty previously described. An overall measurement equipment uncertainty in D_{ij}, or D_{ij}^{eq} when a sample is present in the cell, of 2.30% was found by calculating the RSS of the individual contributions to the uncertainty listed in Table 2.

When using the resistance network method, the experimental uncertainty of the effective diffusion coefficient, D_{ij}^{eff}, is impacted by two sources of error: the measurement equipment uncertainty calculated above and the error due to the use of the resistance network approximation. Dong et al.[23] provides a more detailed analysis of the error associated with the use of a resistance network approximation and how it can be effectively eliminated for a well-designed experiment.

The measurement equipment uncertainty in D_{ij}^{eff} due to the uncertainty in D_{ij}^{eq} can be expressed using Eq. 21, such that

$$\delta D_{ij}^{eff} = \left| \frac{\partial D_{ij}^{eff}}{\partial D_{ij}^{eq}} \delta D_{ij}^{eq} \right| \tag{22}$$

where D_{ij}^{eff} is calculated from the resistance network in Eq. 18. Thus, measurement equipment uncertainty in D_{ij}^{eff} is equal to

$$\delta D_{ij}^{eff} = \left[l \frac{x_p}{(D_{ij}^{eq})^2} \left(\frac{x_p}{D_{ij}^{eq}} - \frac{x_p - l}{D_{ij}^{binary}} \right)^{-2} \right] \delta D_{ij}^{eq} \tag{23}$$

The effect of the measurement equipment uncertainty in D_{ij}^{eff} is strongly influenced by the geometry of the Loschmidt cell, namely the oxygen probe position, x_p, and thickness of the porous sample, l. The geometric sensitivity can be expressed in terms of a resistance ratio, R_{eff}/R_{binary}, which is the ratio of the resistance to diffusion between the sample and the binary gas. Figure 5 shows how the uncertainty due to the measurement equipment varies with the resistance ratio. For many thin materials used in fuel cells such as the gas diffusion layer, microporous layer, and catalyst layer, the resistance ratio can be controlled for a given experiment by stacking multiple samples on top of one another to change the thickness, l. For most practical experiments dealing with submillimeter thick samples, the resistance ratio falls in the range of 0–1 due to physical limitations in probe placement within the cell. Figure 5 shows that the measurement uncertainty is less than 10% when resistance ratio is maintained in this study above 0.5.

For comparison, the resistance ratio for the GDL diffusivity measurements performed by Zamel et al.[11] using a Loschmidt cell is on average 0.075 based on their reported dimensions. Figure 5 shows that this corresponds to a measurement uncertainty of about 30%. Using the same apparatus, PEMFC catalyst layer diffusivity measurements performed by Shen et al.[22] have a resistance ratio that is also about 0.075. However, the substrate that the catalyst layer is applied to results in an additional uncertainty term, which makes the calculation of overall uncertainty less straight forward. Using Eq. 21, the uncertainty was found to be about 60%. These large experimental uncertainties underscore the importance of controlling the resistance ratio in an experiment to achieve accurate measurements.

There are sources of error that have no way of being intentionally perturbed, nor their effect easily measured. The magnitude of some of these errors was calculated by Tordai[35] to show their negligible effect on the results. In other cases, the errors may be excluded from the calculation of uncertainty when the terms appearing in Eq. 21 are at least three times smaller than the largest term.[34] The nil effect of these terms is a result of applying the RSS method, which causes small terms to have very small effects. These sources of error include the following

- An unequal volume of gas in the upper and lower chambers due to valve attachments. The number of valve attachments was reduced compared to the similar apparatus used in Refs. 11, 22, 26, and 28.
- A small initial pressure difference between the gases in the upper and lower chambers can cause an initial mass flux at $t = 0$ that is not due to diffusion. Operating the Loschmidt cell at atmospheric pressure and venting the chamber to atmosphere during chamber filling ensured that no pressure difference would be present.
- The oxygen concentration profile in the Loschmidt cell is assumed from an oxygen sensor measurement at a single-stationary probe location. The accuracy of the probe location, x_p, is essential for predicting the correct oxygen concentration profile. Once the sensor's probe was mounted in the cell, a micrometer depth gauge was used to measure its location. The uncertainty in the distance from the midplane is estimated as ± 0.1 *mm*. However, this measurement does not influence the overall uncertainty of D_{ij}^{eff} because the systematic error remains constant for both measurements of

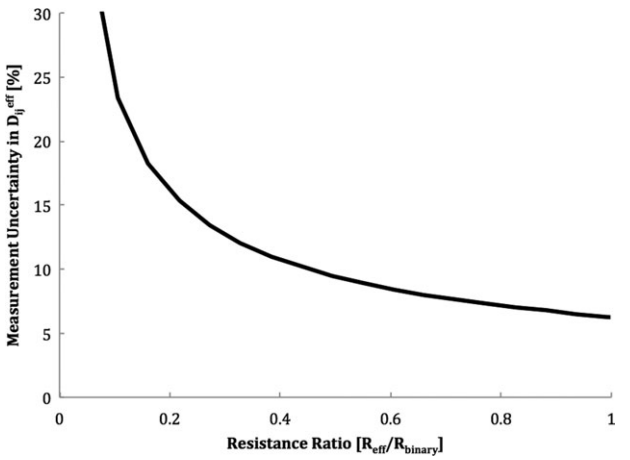

Figure 5. Measurement uncertainty for the effective diffusion coefficient, D_{ij}^{eff}, as a function of resistance ratio.

In this study, uncertainty is less than 10% for a resistance ratio above 0.5.

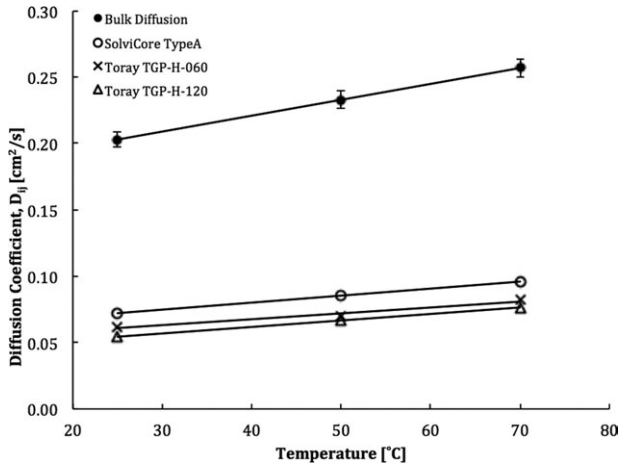

Figure 6. Binary gas diffusion coefficient and effective diffusion coefficient of gas diffusion layers measured at various temperatures using the Loschmidt cell developed in this study.

Each data point is an average of 3 measured samples.

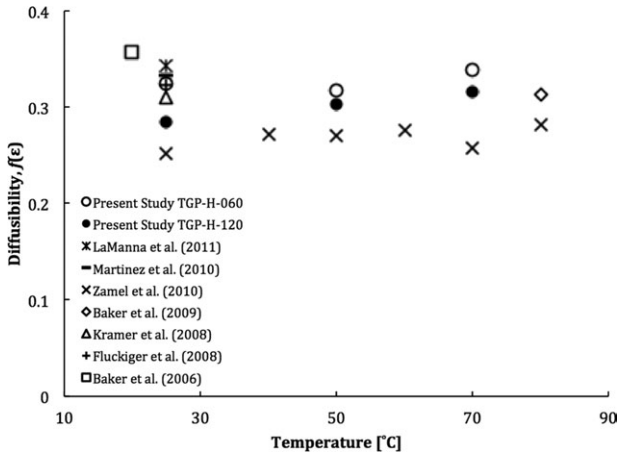

Figure 7. Diffusibility of Toray gas diffusion layer experimentally determined by various studies over a range of temperatures with no (or minimum) compression force applied.

D_{ij}^{binary} and D_{ij}^{eq}. By applying Eq. 18 to solve for D_{ij}^{eff}, the systematic error in x_p is cancelled out.

- At the start of a measurement, the sliding gate spends several seconds in a partially open position during its opening movement. Tordai[35] showed that this event would generate a constant time error. Similarly, the oxygen sensor has a manufacturer reported response time of less than 1 s that generates a time error. These errors do not affect the shape of the oxygen concentration vs. time profile; they only shift it along the time axis. The precise start time of the experiment, $t = 0$, is found by extrapolating the oxygen concentration measured by the sensor vs. time data to the time when oxygen concentration equals zero in Figure 2. The stepper motor controller aids in the repeatability of this event.
- The opening movement of the sliding gate can introduce a perturbation in the fluid. This effect has been investigated and shown to be small.[35] Performing measurements with various gate opening speeds have confirmed this result.
- Errors due to convective mass flux have been minimized through apparatus design. The lighter gas, nitrogen, is placed in the upper chamber to prevent buoyancy effects from driving the flow. Similarly, the Loschmidt cell is mounted vertically, rather than horizontally, to prevent a "spillage" convective flux where the heavier gas spills into the opposite chamber.
- The Loschmidt cell has been mounted on rubber dampers to minimize the effect of vibrations on the experiment. High frequency vibrations can increase the rate that gases mix and influence the measurement of diffusive flux.

Table 3. Diffusibility of Gas Diffusion Layers Measured at Various Temperatures

	Diffusibility ($D_{ij}^{eff}/D_{ij}^{binary}$)		
Temperature (°C)	Toray TGP-H-060	Toray TGP-H-120	SolviCore TypeA
25	0.324	0.284	0.377
50	0.317	0.303	0.389
70	0.339	0.316	0.396
Average	0.327	0.301	0.387

- Temperature gradients are eliminated through the manifold design discussed in Section Temperature. Thermocouples mounted in the upper and lower gas chambers confirm a negligible temperature difference.
- The absorption and desorption of gases in the sliding gate sealing o-rings and lubricant can dilute the concentration gradient. Experiments were performed to quantify the rate of adsorption and desorption, measured with the oxygen sensor. Measurement runtime was chosen to minimize this error, while still collecting enough data points to not compromise measurement accuracy.

Results and Discussion

Effect of temperature

The effect of temperature on nitrogen-oxygen diffusion has been extensively measured in literature.[21,25] Figure 6 presents the binary gas diffusion measurements from this study with error bars that show the experimental uncertainty calculated in Section Uncertainty Analysis. The measurements agree well with those in literature and fall within the uncertainty limits described in each. This agreement helps to validate the results presented in this study.

The GDL is comprised of graphitized carbon fibers that are dimensionally stable within the temperature range evaluated in this study. Thus, it is expected that diffusibility will not change with temperature. The measured through-plane GDL diffusibility is summarized in Table 3 for different temperatures. Diffusibility increases slightly with temperature; however, the increase is within the bounds of experimental error. This is in agreement with the experimental results of Zamel et al.[11] An average diffusibility is provided in Table 3 as a best estimate of diffusibility.

Comparison to existing literature

Several research groups have measured the diffusibility of untreated Toray GDL using the techniques of limiting current, water evaporation, electrochemical diffusimetry, and the Loschmidt cell.[10,11,13–15,18] It is a useful exercise to compare the results from these studies to determine whether they are in agreement. Figure 7 presents the measured diffusibility of various Toray GDL (−030, −060, −090, and −120 series) reported in literature as a function of the temperature

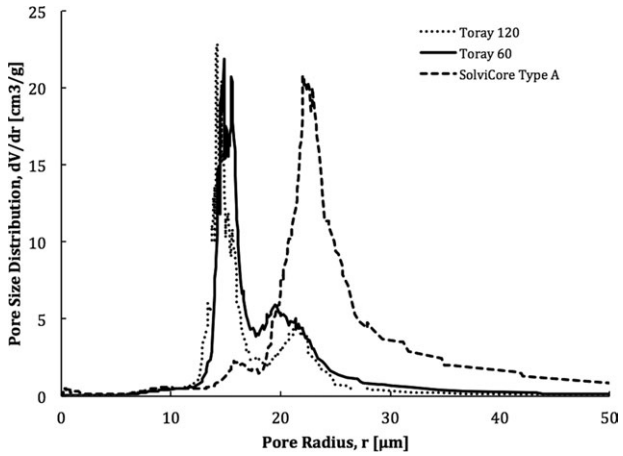

Figure 8. Pore-size distributions of gas diffusion layers found by the MSP.

they were measured at. Using the average of each research group's measurements, the average diffusibility for Toray GDL in literature is 0.317 at no compression. The results of this study agree well with others.

Effect of GDL microstructure

GDL Thickness A common assumption in current literature is that GDLs within the same series (i.e., Toray GDL −030, −060, −090, and −120 series) have a uniform microstructure that is independent of manufactured thickness. In general, this assumption is made so that the thickness of a GDL can be varied within an experiment. The diffusibility of Toray TGP-H-060 and TGP-H-120 have not been measured with the same experimental apparatus. For example, Kramer et al.[10] measured the diffusibility of only TGP-H-060 and Zamel et al.[11] measured the diffusibility of only TGP-H-120. Between the two experimental techniques, measurement uncertainty is too large to directly compare the diffusibility. This is further evidenced in Figure 7, which shows a wide range of measured values for Toray GDL.

The diffusibility of Toray TGP-H-060 and TGP-H-120 differ by 8% in Table 3, which suggests that the microstructure of the two Toray GDLs are not the same. This result is supported by differences in porosity recorded in Table 1. Fishman et al.[36,37] used high-resolution computed tomography to show that TGP-H-060 and TGP-H-120 have a heterogeneous through-plane porosity distribution. TGP-H-060 exhibited a higher porosity in the core region of the GDL, and a lower porosity near the edges. Interestingly, TGP-H-120 had a through-plane porosity distribution that resembles two TGP-H-060 GDL stacked together. This suggests that thicker Toray GDLs are manufactured by compressing multiple plies together.[1,38] Similarly, TGP-H-090 is believed to be comprised of three layers of TGP-H-030.[39]

The heterogeneous porosity distributions of Fishman *et al.*[36,37] agree well with the pore-size distributions in Figure 8 for Toray TGP-H-060 and TGP-H-120. Pore size in these GDLs fall into two distinct groups around 12–17 μm and 18–24 μm, corresponding to near surface and core regions of the GDL, respectively.

Figure 8 and knowledge of the manufacturing differences between Toray TGP-H-060 and TGP-H-120 can help to explain why TGP-H-120 has a lower diffusibility than TGP-H-060. The force applied to the TGP-H-120 to mold the plies together reduces the porosity of the subsequent GDL. Figure 8 shows that the TGP-H-120 has fewer pores in the 18–24 μm range than the TGP-H-060. Large pores, corresponding to a large distance between fibers, are the mechanically weakest part of the GDL. As a result, compression force will have the largest effect on these large pores as Figure 8 demonstrates.

These results are significant for studies that assume uniformity between different manufactured thicknesses to infer aspects on how a PEM fuel cell operates. Caution should be used when small property variations, such as an 8% difference in diffusibility, between Toray TGP-H-060 and TGP-H-120 could impact the accuracy of the measurements. In literature, thermophysical property measurements are commonly expressed or implied to have uncertainties of less than 8%.

GDL Manufacturer This study is the first to the authors' knowledge to measure the diffusibility of SolviCore Type A GDL, provided in Table 3. The most appropriate comparison to the diffusibility of SolviCore can be made with Toray TGP-H-060, of which both are near identical thickness. Diffusibility of the SolviCore GDL is ∼20% greater than Toray TGP-H-060. This result can be attributed to the porosity and pore-size distribution of the respective GDL. The porosity of the SolviCore GDL is ∼8% greater than the TGP-H-060. Although pore size ranges from 13–30 μm for the TGP-H-060 GDL, pore size for the SolviCore GDL have a much larger range of 13–50 μm.

In-plane SEM images of SolviCore and Toray GDLs are presented in Figures 9 and 10, respectively. The primary microstructure differences between the two GDLs are in the fiber arrangement and the distribution of binder between the fibers.

Fibers in the Toray GDL are tightly stacked on top of one another in the through-plane direction. The inlay in Figure 10 shows at least eight fibers stacked above one another. Considering these eight overlapping fibers are all within the depth of focus of the camera, this suggests that they are in close proximity to one another. In contrast, the fibers of the SolviCore GDL are more spread out in the through-plane direction. The inlay in Figure 9 shows only two overlapping fibers within the depth of focus of the camera, with a third fiber out of focus in the background. This suggests that there

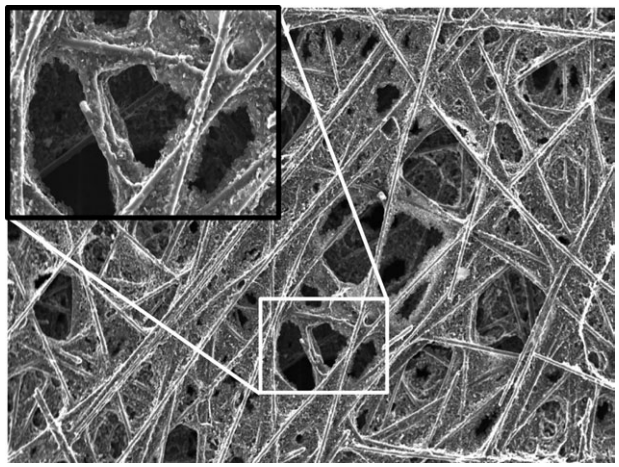

Figure 9. In-plane SEM image of SolviCore Type A gas diffusion layer at 100x magnification.

Inlay shows enlarged region of interest.

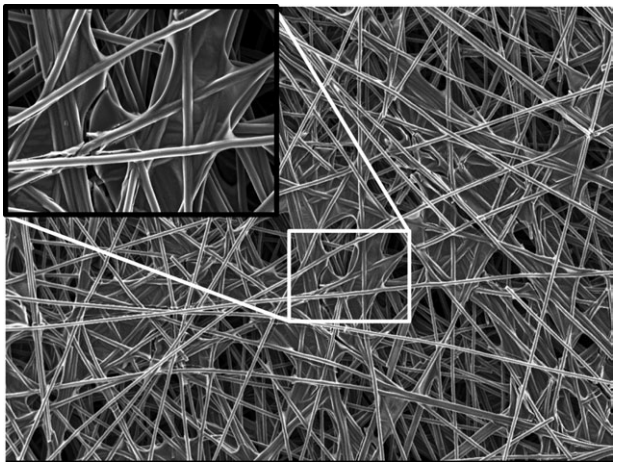

Figure 10. In-plane SEM image of Toray TGP-H-060 gas diffusion layer at 100x magnification.

Inlay shows enlarged region of interest.

is a mat of fibers in the foreground and another in the distance, separated by a large void space or pore.

There is significantly more binder per fiber visible in the SolviCore GDL than the Toray GDL in Figures 9 and 10. The binder in the Toray GDL forms smooth skins between the fibers, distinctly different from the coarse particles of the SolviCore GDL binder. Kramer et al.[10] notes that the skins are preferentially oriented in the in-plane direction. The binder distribution of the SolviCore resembles clumps around the fibers without being preferentially oriented in any direction.

Limitations of current geometric models

It has been well demonstrated in current literature that relevant correlations based on porosity significantly over predict the through-plane diffusibility of carbon papers.[7,10–12,18] The primary shortfall with these correlations is that they do not take into account the amount and distribution of binder on the fibers. In fact, correlations agree very well with experimental data for carbon cloths,[12] which do not contain any binder material.

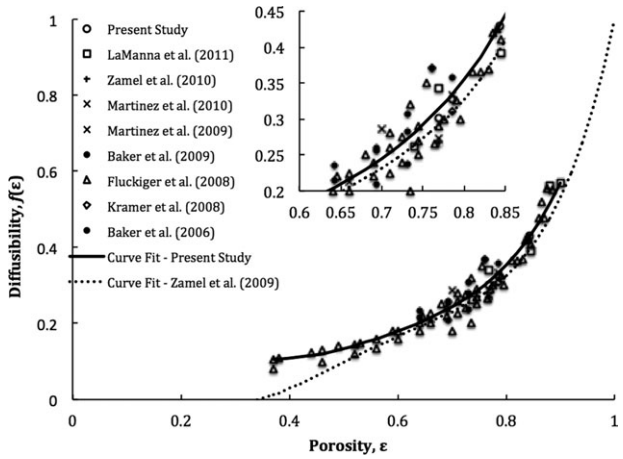

Figure 11. Diffusibility of gas diffusion layers with less than 10%-wt.

PTFE content as a function of porosity that have been reported in literature.

Including an additional parameter in a geometric model that considers the amount of binder present could provide better agreement between geometric models and experimental data. Figures 9 and 10 show that binder has a significant impact on the shape, orientation, and effective length of pores based on the amount and distribution of binder on the fibers. As such, the tortuosity parameter, τ, in a geometric model should be a function of the binder content. However, tortuosity cannot be determined by straight forward means making the influence of the binder difficult to quantify.

Correlations developed from experimental data alleviate the difficulties in quantifying the influence of the binder on diffusibility, because the experimental measurements inherently include them. Zamel et al.[7] developed a correlation for the diffusibility of Toray GDL as a function of porosity using a geometric model that was validated using experimental data. However, their model is not necessarily applicable to other brands of GDL because the distribution of binder varies significantly from one brand of GDL to another (Figures 9 and 10). At the time of publication, experimental data for other GDL brands were not available.

Modified correlation using experimental data

Figure 11 provides diffusibility measurements for GDL with less than 10% PTFE content from several studies as a function of porosity, presented together for comparison. The inlaid graph provides an enlarged region of the data for clarity. The data shows a distinct trend despite have a relatively large spread, which is attributed to the high measurement uncertainty in the respective studies, and the variations in microstructure among GDL manufacturers.

Using the correlation developed by Das et al.,[6] Eq. 4, and the geometric factor developed by Zamel et al.,[7] Eq. 5, a new set of correlation parameters is found using the experimental data in Figure 11. Table 4 presents the correlation parameters generated from a least-squares fit with an R^2 value of 0.933, compared to the values used by Zamel et al.[7] that results in an R^2 value of 0.887 for this set of experimental data. Thus, the modified correlation for the through-plane GDL diffusibility as a function of porosity is

$$f(\epsilon) = \left(1 - (2.72\epsilon)\cosh(2.53\epsilon - 1.61)\left(\frac{3(1-\epsilon)}{3-\epsilon}\right)\right) \quad (24)$$

Equation 24 is shown in Figure 11, along with the original correlation proposed by Zamel et al.[7] Although the original correlation gives a reasonable estimate of diffusibility for porosities between 0.6 and 0.9, below this range it deviates greatly.

Equation 24 provides the best estimate to date of diffusibility as a function of porosity for all GDLs with less than

Table 4. Correlation Parameters for Eq. 24 that Predict the Through-Plane Diffusibility of Gas Diffusion Layers with less than 10%-wt PTFE content

	A	B	C	Validity Range	R^2
Zamel et al. (2000)	2.76	3.00	1.92	$0.33 \leq \epsilon \leq 1.0$	0.887
Present Study	2.72	2.53	1.61	$0.37 \leq \epsilon \leq 0.9$	0.933

10%-wt. PTFE. A precise correlation may not be feasible to describe the through-plane diffusion in all GDL carbon papers due to the diversity in microstructure present among different GDL manufacturers. However, future studies may benefit from this work for estimating GDL diffusibility in fuel cell models where precise experimental data does not exist. The experimental methods developed in this work, particularly with regards to measurement uncertainty, should lead to more accurate diffusibility measurements for GDL, as well as measurements on the diffusibility of the microporous layer and catalyst layer of PEMFCs for which there is limited data.

Conclusion

In this study, the closed-tube method, commonly referred to as the Loschmidt cell, was modified to measure the effective diffusion coefficient of submicrometer thick samples to a high degree of accuracy. Improvements over previous Loschmidt cell designs were achieved by identifying parameters sensitive to measurement error. A resistance ratio was identified as an important parameter that affected uncertainty and stacking multiple samples during measurement allowed this parameter to be controlled. The effective diffusion coefficient was measured for Toray and SolviCore GDL and the effect of thickness and microstructure was assessed. Diffusibility varied with thickness for Toray GDL, with a difference of 8% between the samples tested. This breaks the standing assumption that transport coefficients are the same at different thicknesses. The SolviCore GDL had a 20% greater diffusibility than Toray GDL, which was attributed to the substantially larger pores of the SolviCore GDL. Experimental diffusibility results in published literature covering a variety of measurement techniques were presented together as a function of porosity. A modified correlation that relates diffusibility to porosity for carbon paper GDL with less than 10%-wt. PTFE was proposed that takes into account all of this experimental data. The correlation should prove useful for the estimation of diffusion coefficients in fuel cell models when specific experimental data are not available.

Acknowledgments

The financial support from AUTO21 Network of Centres of Excellence and Natural Sciences and Engineering Research Council (NSERC) of Canada is gratefully acknowledged. In addition, the authors thank SolviCore GmbH for providing the SolviCore GDL samples used in this study.

Literature Cited

1. Vielstich W, Lamm A, Gasteiger H. *Handbook of Fuel Cells — Fundamentals, Technology and Applications*. New York: John Wiley and Sons, 2003.
2. Ho C, Webb S. *Gas Transport in Porous Media*. Dordrecht, Netherlands: Springer, 2006.
3. Volfkovich Y, Bagotzky V. The method of standard porosimetry: 1. principles and possibilities. *J Power Sources*. 1993;48:327–338.
4. Bear J. *Dynamics of Fluids in Porous Media*. New York: Dover Publications, 1972.
5. Bruggeman D. Calculation of various physics constants in heterogenous substances: dielectricity constants and conductivity of mixed bodies from isotropic substances. *Ann Phy*. 1935;24:636–664.
6. Das P, Li X, Liu Z. Effective transport coefficients in PEM fuel cell catalyst and gas diffusion layers: beyond Bruggeman approximation. *Appl Energy*. 2010;87:2785–2796.
7. Zamel N, Li X, Shen J. Correlation of the effective gas diffusion coefficient in carbon paper diffusion media. *Energy Fuels*. 2009;23:6070–6078.
8. Tomadakis M, Sotirchos V. Ordinary and transition regime diffusion in random fiber structures. *AIChE J*. 1993;39:397–412.
9. Tomadakis M, Robertson T. Viscous permeability of random fiber structures: comparison of electrical and diffusional estimates with experimental and analytical results. *J Compos Mater*. 2005;39:163–188.
10. Kramer D, Freunberger S, Flückiger R, Schneider I, Wokaun A, Büchi F, Scherer G. Electrochemical diffusimetry of fuel cell gas diffusion layers. *J Electroanal Chem*. 2008;612:63–77.
11. Zamel N, Astrath N, Li X, Shen J, Zhou J, Astrath F, Wang H, Liu Z. Experimental measurements of effective diffusion coefficient of oxygen-nitrogen mixture in PEM fuel cell diffusion media. *Chem Eng Sci*. 2010;65:931–937.
12. Martínez M, Shimpalee S, Van Zee J. Measurement of MacMullin numbers for PEMFC gas-diffusion media. *J Electrochem Soc*. 2009;156:B80–B85.
13. LaManna J, Kandlikar S. Determination of effective water vapor diffusion coefficient in PEMFC gas diffusion layers. *Int J Hydrogen Energy*. 2011;36:5021–5029.
14. Baker D, Wieser C, Neyerlin K, Murphy M. The use of limiting current to determine transport resistance in PEM fuel cells. *ECS Trans*. 2006;3:989–999.
15. Baker D, Caulk D, Neyerlin K, Murphy M. Measurement of oxygen transport resistance in PEM fuel cells by limiting current methods. *J Electrochem Soc*. 2009;156:B991–B1003.
16. Beuscher U. Experimental method to determine the mass transport resistance of a polymer electrolyte fuel cell. *J Electrochem Soc*. 2006;153:A1788–A1793.
17. Stumper J, Haas H, Granados A. In situ determination of MEA resistance and electrode diffusivity of a fuel cell. *J Electrochem Soc*. 2005;152:A837–A844.
18. Flückiger R, Freunberger S, Kramer D, Wokaun A, Scherer F GG Büchi. Anisotropic, effective diffusivity of porous gas diffusion layer materials for PEFC. *Electrochim Acta*. 2008;54:551–559.
19. Martínez M, Tong C, Shimpalee S, Van Zee J. Characterization of microporous layer in carbon paper GDL for PEM fuel cell. *ECS Trans*. 2010;33:1133–1141.
20. Chan C, Zamel N, Li X, Shen J. Experimental measurement of effective diffusion coefficient of gas diffusion layer/microporous layer in PEM fuel cells. *Electrochim Acta*. 2012;65:13–21.
21. Marrero T, Mason E. Gaseous diffusion coefficients. *Phys Chem Ref Data*. 1972;1:3–118.
22. Shen J, Zhou J, Astrath N, Navessin T, Liu Z, Lei C, Rohling J, Bessarabov D, Knights S, Ye S. Measurement of effective gas diffusion coeffcients of catalyst layers of PEM fuel cells with a Loschmidt diffusion cell. *J Power Sources*. 2011;196:674–678.
23. Dong L, Unsworth G, Li X. Errors and uncertainty in diffusion measurements through thin porous media. In press.
24. Loschmidt J. Experimental-Untersuchungen uber die Diffusion vonGasen ohne porose Scheidewande. *Wiener Berichte*. 1870;61:367–380.
25. Marrero T, Mason E. Temperature dependence of gaseous diffusion coefficients. *Chem Eng Commun*. 1980;7:159–168.
26. Rohling J, Shen J, Wang C, Zhou J, Gu C. Determination of binary diffusion coefficients of gases using photothermal deflection technique. *Appl Phys B: Lasers Opt*. 2007;87:355–362.
27. Rohling JH, Shen J, Wang C, Zhou J, Gu CE. Photothermal deflection measurement of effective gas diffusion coefficient of a porous medium. *Eur Phys J - Special Topics*. 2008;153:111–113.
28. Astrath N, Shen J, Song D, Rohling J, Astrath F, Zhou J, Navessin T, Liu Z, Gu C, Zhao X. The effect of relative humidity on binary gas diffusion. *J Phy Chem*. 2009;113:8369–8374.
29. Astrath NGC, Shen J, Astrath FBG, Zhou J, Huang C, Yuan XZ, Wang H, Navessin T, Liu ZS, Vlajnic G, Bessarabov D, Zhao X. Note: determination of effective gas diffusion coefficients of stainless steel films with differently shaped holes using a Loschmidt diffusion cell. *Rev Scientific Instruments*. 2010;81:046104–046104–3.
30. Ocean Optics Inc. *NeoFox Installation and Operating Manual*. Dunedin, FL: Ocean Optics, 2010.
31. Kautsky H. Quenching of luminescence by oxygen. *Trans Faraday Soc*. 1939;35:216–219.
32. Toray Industries Inc. Carbon Paper Specifications, 2005. URL http://www.torayca.com/en/index.html. Accessed May 2012.
33. Crank J. *The Mathematics of Diffusion*. Bristol, UK: Oxford University Press, 2nd ed. 1975.

34. Moffat R. Describing the uncertainties in experimental results. *Exper Ther Fluid Sci*. 1988;1:3–17.
35. Tordai L. Errors in diffusion measurements by the Loschmidt method. *Bri J Appl Phys.* 1950;1:329–332.
36. Fishman Z, Hinebaugh J, Bazylak A. Microscale tomography investigations of heterogeneous porosity distributions of PEMFC GDLs. *J Electrochem Soc*. 2010;157:B1643–B1650.
37. Fishman Z, Bazylak A. Heterogeneous through-plane distributions of tortuosity, effective diffusivity, and permeability for PEMFC GDLs. *J Electrochem Soc*. 2011;158:B247–B252.
38. Gao B, Steenhuis T, Zevi Y, Parlange J, Carter R, Trabold T. Visualization of unstable water flow in a fuel cell gas diffusion layer. *J Power Sources*. 2009;190:493–498.
39. Maheshwari P, Mathur R, Dhami T. The influence of the pore size and its distribution in a carbon paper electrode on the performance of a PEM Fuel cell. *Electrochim Acta*. 2008;54: 655–659.

Manuscript received Jun. 21, 2012, and revision received Aug. 7, 2012.